Modeling and Analysis of a Flexible End-effector for Actuating Endoscopic Catheters

K. P. Ashwin* Don. P Jose† Ashitava Ghosal‡
Indian Institute of Science
Bangalore, India

Abstract—*Precise positioning of catheters during an endoscopic procedure and surgery is typically a very complex and demanding task. Once endoscope tip is stationed at a particular position, the camera is focused at a particular point. In most endoscopes, any motion of the catheter is achieved by moving the endoscope tip which results in a change in camera focus. This paper presents an innovative end-effector design which may be used alongside a camera in such a way that independent motion of catheter is achieved. The design utilizes the advantages of miniaturized pneumatic artificial muscles (MPAM) with a diameter less than 1.2 mm. Three such MPAMs are arranged in a manner so that the tip of the end-effector can be moved by over 15 mm in three-dimensions. This paper presents the detailed design, characteristics of MPAM used, kinematics of end-effector and hardware implementation used to achieve arbitrary tip motion of the end-effector.*

Keywords: McKibben air muscle, miniaturized pneumatic actuators, minimally invasive surgical tools, soft robotics

I. Introduction

Endoscopy is a medical procedure in which a long tube called an endoscope is inserted inside a patient's gastro-intestinal tract typically for diagnosis. Similar procedures called colonoscopy is used for examination of the colon. In these procedures, a standard flexible endoscope contains a camera, a fibre optic based illumination and image capture system, air-water channels and nozzle for removing obstacles all enclosed in a flexible tube of about 7 to 15 mm diameter. Almost all commercially available endoscopes also carry a channel through which an instrument (catheter) can be introduced at the distal end. The instrument (catheter) can be operated by the doctor/technician from the dorsal end (holding end) of the endoscope. Depending on the different types of catheters, endoscopy can also be used for extracting tissue for biopsy, some forms of treatments as well as surgery. However, in most commonly available endoscopes, once a catheter is introduced at the distal end, the independent motion of catheter from camera is not possible—the endoscopists are not able to move the catheter laterally while keeping the camera stationary.

*ashwinkp@mecheng.iisc.ernet.in
†jose.donabc@gmail.com
‡asitava@mecheng.iisc.ernet.in

A few commercially available endoscope platforms used for natural orifice translumenal endoscopic surgery address this issue[1]. These are either very expensive and do not often use the same standard catheters available in the market. Conventional actuation techniques are not quite suitable in actuating endoscopic catheters since both precise control and flexibility are desired at a miniature size. At present, the tip of endoscope is moved by pulling a set of strings(tendons), as in [2], which actuates a series of universal joints. This technique cannot be easily applied for actuating catheter since the load carrying capacity is very low. Also, the end-effector in actuated position needs to be compliant against external forces—like when endoscope presses against the side walls of GI tract—so that chances of endoscope tearing tissues ('perforation') are minimized. The conventional tendon-driven mechanisms might not be able to exhibit required compliance in actuated position. The use of micro-motors is ruled out since it increases the weight at the tip of endoscope apart from making the end of the endoscope rigid. Shape memory alloy (SMA) wires have the required flexibility and precise positioning capability[3, 4, 5]. However, the response time of SMA wires are large (of the order of tens of seconds) and in some instances the temperature increase due to heating of SMA wires for their actuation is not desirable. McKibben actuator/ Pneumatic Air Muscle(PAM), actuated by pressurized fluid, are promising actuators due to two principal advantages: soft and highly flexible when not pressurized and stiff and large load carrying capacity when pressurized[6], [7]. A McKibben actuator/PAM consists of a hollow hypeelastic tube/bladder which is braided on the outside using a mesh of inextensible cords. One end of the tube/bladder is sealed and compressed air is allowed to enter through the other end. The tube/bladder in its normal unpressurized state is soft and very flexible. Upon pressurizing, the tube/bladder inflates while the inextensible mesh on the outer surface limits the expansion to a particular volume. It can be shown that if the initial angle of winding of a cross-mesh (braiding) is less than $54.7°$, the air muscle will contract longitudinally and can carry axial load while it is pressurized [6]. Pneumatic air muscles were first introduced in 1950s, but very little use of these are found for precise positioning. This is primarily due to the unavailability of satisfactory theoretical models and difficulty in control[8]. In this work, we use miniaturized PAM (MPAM) with diame-

ter of 1.2 mm for development of a catheter which can be independently positioned in a two-dimensional region [9]. We present characterization of these MPAMs, a design of a catheter actuated by three MPAMs, and initial attempts at deriving the kinematics of an end-effector and its control.

The paper presents an innovative end-effector design which uses MPAM to actuate commercially available or specially designed catheter for endoscopy. Section II details the end-effector configuration and its design. In section III, MPAM used for moving the end-effector is analyzed for deflection and force generated. In section IV, the kinematics and workspace of end effector is studied for single air muscle actuation and when two air muscles are actuated simultaneously. In section V, the hardware for real-time control of the end-effector and its interfacing with a thumb stick input device is described. In section VI, representative experimental results are reported and the conclusions and scope for future work are presented in section VII.

II. End-effector Design

A CAD model as well as the fabricated end-effector is shown in Fig.1 and Fig.2 respectively. The end-effector consists of two holders on either ends, each having a central hole of 3.5 mm diameter for catheter entry and three holes of 2 mm diameter, 120° apart for placement of MPAMs. The separation between dorsal and distal holders decides the overall length of end-effector and hence the length of the MPAM used. A minimum end-effector deflection of 10 mm is desired for convenient positioning of the tip of a catheter and this is kept as a design target during the fabrication. It has been experimentally observed that air muscle length below 40 mm does not produce a large enough force to bend standard forceps catheter to required deflection[9]. In addition, since the depth of view of a typical endoscopic camera is between 0 to 90mm, a 45 mm length of the air muscles was chosen in the design.
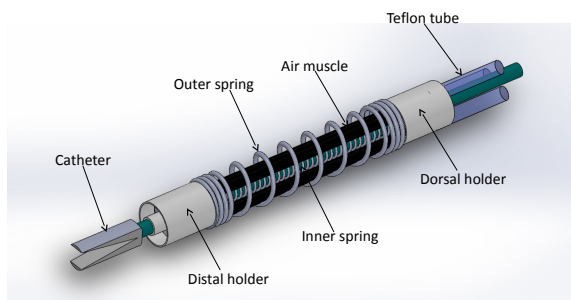

Fig. 1. Components of end-effector and CAD model

As shown in Fig. 1, a wound coil of 4 mm outer diameter is fixed in the center. This coil serves two purposes—it acts as a passage for catheter without interfering with the pneumatic air muscles and also acts as a fulcrum on which the catheter will bend when air muscle is energized. The coil is pre-stressed to get high axial stiffness and minimal

motion along the coil—as a consequence the end-effector workspace is a surface. The outer coil is highly flexible and is used to maintain the shape of the end-effector. The pneumatic air muscles are rigidly fixed to the top and bottom holders. While it is sealed at the top holder, the air muscles are connected at the bottom to Teflon tubes of 2 mm diameter which in turn is connected to a compressed air reservoir. In its current form (see figure 2), the end-effector is 55 mm long and has a diameter of 9 mm. Fig. 3 shows the lay-

Fig. 2. End-effector with forceps

out of pneumatic circuit used to actuate the end-effector. A compressor with an output capacity of up to 1034 kPa (150 psi) is connected to a reservoir and a pressure regulator system keeps the air pressure in reservoir at about 827 kPa (120 psi) at all times. This compressed air is delivered to air muscle using three pairs of Parker VSO series proportional valves (denoted as S1-S6)[10]. The valves S1, S3, S5 are used to regulate air flow into the muscle while S2, S4 and S6 are used for bleeding air to the atmosphere. A controller receives feedback of the pressure from three Honeywell pressure transducers (denoted as PS1, PS2 and PS3 in the figure) in the range 0 to 1034 kPa (150 psi) and drives the valves so as to maintain required pressure inside the air muscle. The set up uses an Arduino Mega 2560 board[11] interfaced with MATLAB [12] for the entire controller instrumentation. Since the proportional valves are current based and the Arduino is unable to supply the required current, a current driver circuit is used and the valves can be driven using Arduino board's analog voltage output [9].

III. Characterization of MPAM

Deflection versus axial force on a 45 mm MPAM with 758.4 kPa (110 psi) pressure is shown in Fig. 4. As an initial approximation, polynomial curve was fitted on the data. It can be seen that a cubic fit gives a very close approximation to the experimental data. The main drawback of curve fitting on experimental data over an analytical model is its limited use in controller design. However, as described in [8], till now there are no definitive static models available in the literature for McKibben actuators. The earlier mathe-
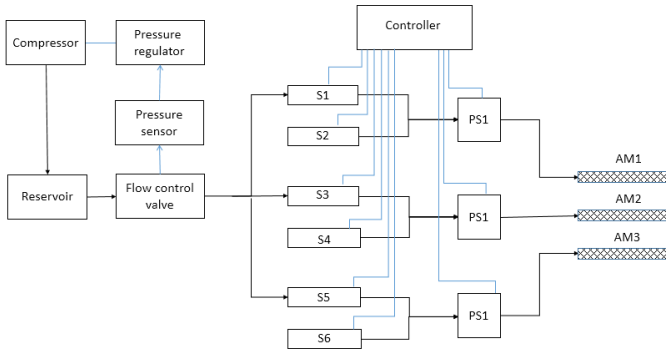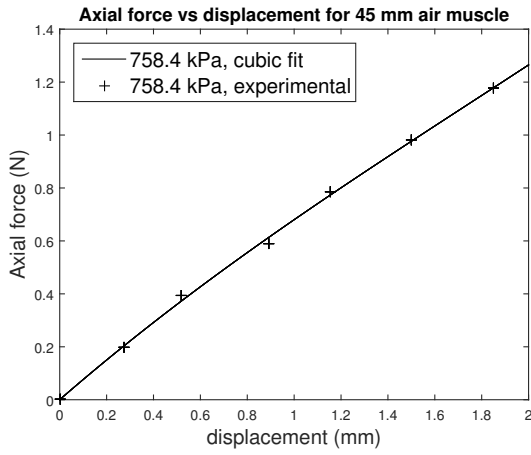
Fig. 3.   Layout of pneumatic circuitry

Fig. 4.   Cubic fit on experimental data

matical models by Schulte[13] and Chou-Hannaford[6] deviate from experimental results by more than 20% for the MPAM under consideration. One possible reason for the discrepancy could be the idealized assumption in their models that cylindrical air muscle remains cylindrical even after pressurizing—this is not true for the MPAM used. In addition, the material properties are not considered in their model.

An attempt on modeling McKibben actuators as fiber reinforced elastic membrane (as given in [14]) was conducted by Liu and Rahn[15]. In their work, the authors find an iterative solution to the equilibrium equations

$$\frac{d\left(\lambda_2 n_2\right)}{d\lambda_2} = n_1 \tag{1}$$

$$\frac{n_1 \cos \sigma}{\lambda_2} + n_2 \frac{d \cos \sigma}{d\lambda_2} = \frac{PR}{2C} \tag{2}$$

Subject to boundary conditions

$$\lambda_{(L)} = 1 \tag{3}$$

$$n_{2(0)} = \frac{PR\lambda_{2(0)}}{4C} + \frac{F}{4\pi CR\lambda_{2(0)}} \tag{4}$$

$$\sigma_{(0)} = 0 \tag{5}$$

to obtain the deformed shape of a pressurized actuator. In the above equation, P is the pressure inside the tube, R is the initial radius, C is Mooney-Rivlin constant, σ is the slope of meridian, λ_1, λ_2 are the stretch ratios in the axial and lateral direction, n_1, n_2 are the stress per unit length in axial and lateral direction.

The iterative procedure considers an initial value of $\lambda_{2(0)}$ and proceeds towards finding pressure P and thereby the deformed shape. In our case, $P_{(0)}$ is a known quantity while $\lambda_{2(0)}$ remains unknown and hence, the procedure had to be modified. The results obtained for a 45 mm long 1.74 mm diameter MPAM with 620.5 kPa (90 psi) and 758.4 kPa (110 psi) applied pressure is shown in Fig. 5. The solution from the iterative formulation is plotted alongside experimental results for comparison. It can be seen that the trend is similar, with a maximum error of 1.6 mm in deflection. It maybe mentioned that the iterative solution procedure carried out in MATLAB takes about 74 seconds to complete.
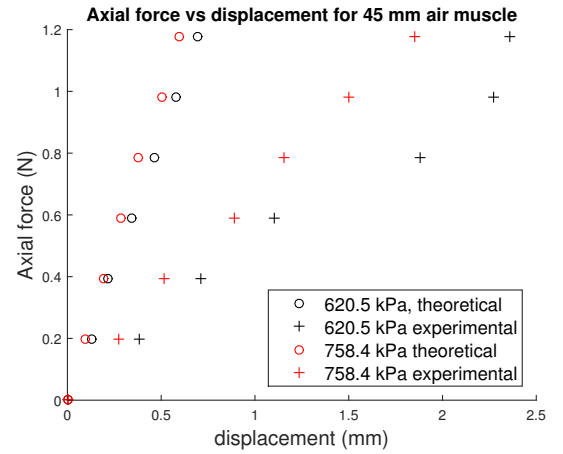

Fig. 5.   Fiber elastic membrane model comparison

IV. Kinematics of end-effector

In this section, we present initial attempts at deriving the kinematics of the end-effector constructed using three MPAMs. The relationship between the applied pressure and deflection of the end-effector is obtained when a single or two MPAMs are pressurized. The workspace of the fabricated end-effector is also obtained.

A. Single air muscle actuation

A single air muscle is pressurized to analyze the maximum displacement of end-effector without the catheter. Since the air muscle is offset from the end-effector axis by a pre-fixed distance, the end effector tip is subjected to a moment which results in bending. In reference[16], the authors show the displacement of elephant trunk robot actuated by pushing and pulling a set of cables placed on either side of a flexible 'backbone'. The length of the cables decide the elephant trunk robot's final shape. The end-effector presented

in this work is similar to the elephant trunk robot with air muscle being analogous to the cables and the inner spring acting like the backbone. However, it should be noted that there are only 3 air muscles in our case and the air muscles contract and become stiffer on application of pressure.
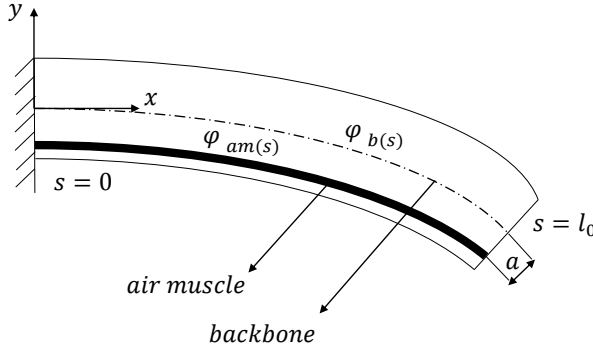

Fig. 6. Analogy with elephant trunk model

From reference[16], we get the expressions for shape of backbone and cables which are deflected in a 2-D plane. These are given as

$$\psi_{b(s)} = \frac{l_0}{\mu} \left(\begin{array}{c} \sin(\mu s) \\ 1 - \cos(\mu s) \end{array} \right) \tag{6}$$

$$\psi_{am(s)} = \frac{l_0}{\mu} \left(\begin{array}{c} \sin(\mu s) \\ 1 - \cos(\mu s) \end{array} \right) + a \left(\begin{array}{c} -\sin(\mu s) \\ \cos(\mu s) \end{array} \right) \tag{7}$$

where $\psi_{b(s)}$ and $\psi_{am(s)}$ represents the position vector of backbone and air muscle respectively, parameter s varies from 0 to l_0 with l_0 denoting the original length of the air muscle, $\mu = \frac{\delta}{2a}$ with δ as the displacement of the air muscle from initial length upon application of pressure, and a is the fixed distance between air muscle and backbone. From the above section, we find $\delta = 14.68$ mm for a 45 mm long air muscle at 827 kPa (120 psi) pressure and $a = 3$mm. Fig. 7 shows the predicted deflection (shown by red backbone and white air muscles) overlapped on actual deflection of end effector. It can be seen that theoretical prediction agrees reasonably well with actual displacement.

The above model could not be used in the case of end-effector with catheter attached due to two possible reasons.
• The coils used for end-effector fabrication has very low transverse stiffness and hence the reaction force experienced on air muscle is very small if catheter is not included. However, once catheter is introduced, the reaction forces are not negligible and the value of forces vary with different catheters used.
• When pressurized, the air muscles other than the one actuated are compressed towards the coil by catheter and
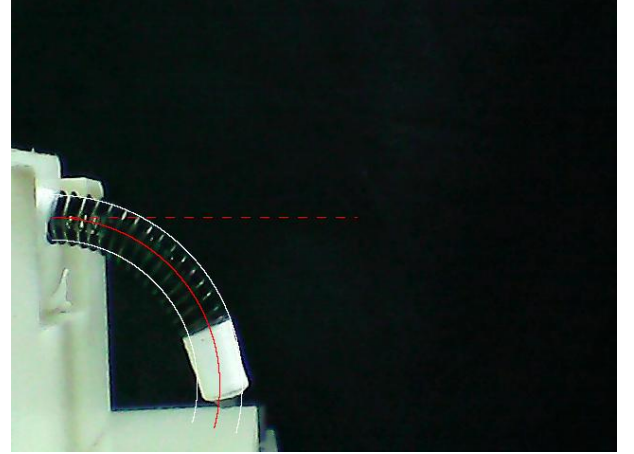

Fig. 7. End effector bending at 827 kPa

hence, a constant value of a is not achieved through out the length of the end-effector.

The deflection of end-effector with a standard 2.5 mm diameter forceps is shown in the Fig. 8. The maximum displacement of ˜22.4 mm is observed at the end of distal holder and ˜26.5 mm at tip of catheter. The pressure versus deflection for single air muscle actuation is plotted in Fig. 9. Due to the unavailability of precise mathematical model, a cubic curve is fitted on experimental data to obtain a relation between pressure and deflection. A pressure of 827 kPa (120 psi) is applied, beyond which negligible change in deflection is observed and is hence set as a maximum limit.
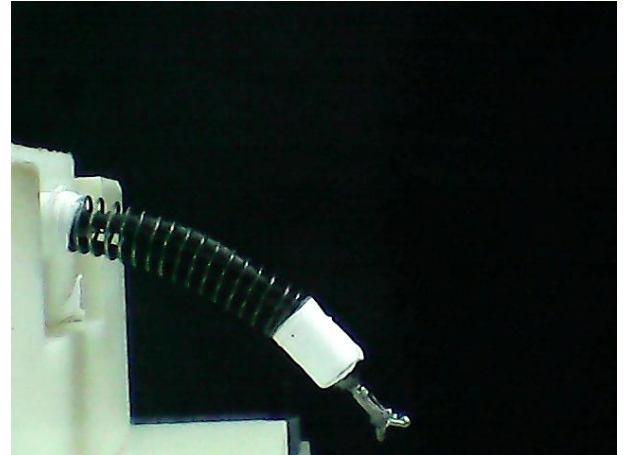

Fig. 8. End effector with forceps at 827 kPa

B. Multiple air muscles actuation
   Fig. 10 shows the front view of the end-effector with three air muscles actuated independently at maximum pressure. Three unit vectors $\mathbf{e}_1, \mathbf{e}_2, \mathbf{e}_3$ represents direction of displacement of air muscles AM1, AM2 and AM3 actuated independently. The workspace spanned by air muscles is shown in Fig. 11 where $A_1\mathbf{e}_1$, $A_2\mathbf{e}_2$, $A_3\mathbf{e}_3$ are
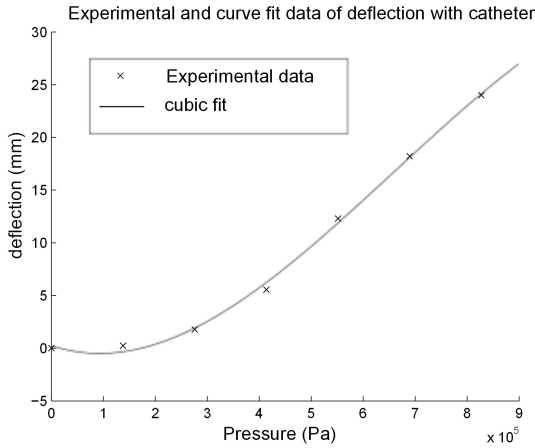
Fig. 9. Pressure vs deflection, with catheter

Fig. 11. Workspace of end-effector

Fig. 10. Front view of end-effector
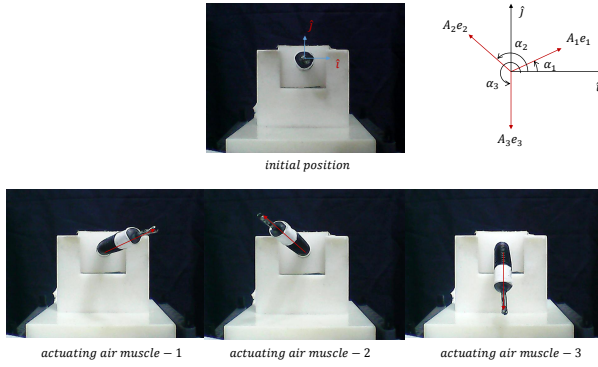

Fig. 12. Vector in workspace

the vectors corresponding to the maximum displacement in $\mathbf{e}_1, \mathbf{e}_2, \mathbf{e}_3$ directions respectively. The sector between $\mathbf{e}_i$ and $\mathbf{e}_j$, $i, j = 1, 2, 3$, $i \neq j$ is termed S_i. To access a particular point in S_i, say $\mathbf{v} = (v_x, v_y)^T$ (see Fig. 12), the air muscles i and j should be pressurized so as to obtain displacements $\mathbf{a}_i$ and $\mathbf{a}_j$ respectively.

From Fig. 11, we get the following set of equations:

$$\begin{bmatrix} \mathbf{e}_i \\ \mathbf{e}_j \end{bmatrix} = \begin{bmatrix} \cos\alpha_i & \sin\alpha_i \\ \cos\alpha_j & \sin\alpha_j \end{bmatrix} \begin{bmatrix} \hat{\mathbf{i}} \\ \hat{\mathbf{j}} \end{bmatrix} \tag{8}$$

$$\begin{bmatrix} \hat{\mathbf{i}} \\ \hat{\mathbf{j}} \end{bmatrix} = \frac{\begin{bmatrix} \sin\alpha_j & -\sin\alpha_i \\ -\cos\alpha_j & \cos\alpha_i \end{bmatrix}}{\sin(\alpha_j - \alpha_i)} \begin{bmatrix} \mathbf{e}_i \\ \mathbf{e}_j \end{bmatrix} \tag{9}$$

$$v_x\hat{\mathbf{i}} + v_y\hat{\mathbf{j}} = \frac{\left\{ \begin{array}{c} v_x\left[\sin\alpha_j\mathbf{e}_i - \sin\alpha_i\mathbf{e}_j\right] \\ + v_y\left[-\cos\alpha_j\mathbf{e}_i + \cos\alpha_i\mathbf{e}_j\right] \end{array} \right\}}{\sin(\alpha_j - \alpha_i)} \tag{10}$$

$$= \begin{array}{c} \left[\frac{v_x\sin\alpha_j - v_y\cos\alpha_j}{\sin(\alpha_j-\alpha_i)}\right]\mathbf{e}_i \\ + \left[\frac{-v_x\sin\alpha_i + v_y\cos\alpha_i}{\sin(\alpha_j-\alpha_i)}\right]\mathbf{e}_j \end{array} \tag{11}$$

$$= a_i\mathbf{e}_i + a_j\mathbf{e}_j \tag{12}$$

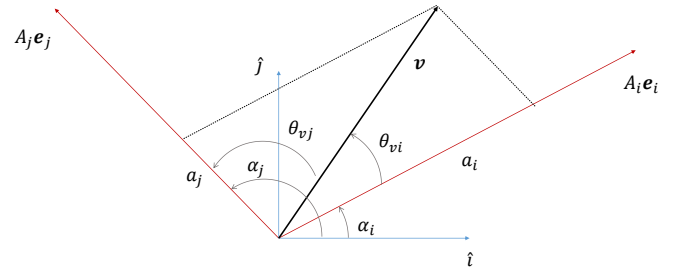The above expression gives the values of a_i and a_j which is

the required displacement from actuators i and j in order to access point (v_x, v_y) in the sector S_i. Fig. 13 and Fig. 14 shows the experimental and expected end-effector position for a pre-defined input. The air muscle AM1 is pressurized at 689 kPa (100 psi) and AM2 is given maximum pressure. It can be seen that the predicted deflection and actual deflection varies by ˜9°.

V. Real-time implementation of end-effector actuation

The actuation of end effector is implemented in real time by taking input from a thumb stick which specifies the desired direction of motion. The analog signal from thumb stick is input to an Arduino Mega board which reads values from 0 to 1024 corresponding to 0 to 5V— (0,0) is the top left corner and (1024,1024) is the bottom right corner. The origin of thumb stick, initially at (512,512) is made (0,0) by using the conversion

$$\begin{array}{rcl} t_x & = & (t_x - 512) \\ t_y & = & -(t_y - 512) \end{array}$$

where (t_x, t_y) are the user input. The analog signals from thumb stick spans a square surface from -512 to +512 in both left-right and top-bottom directions. The workspace
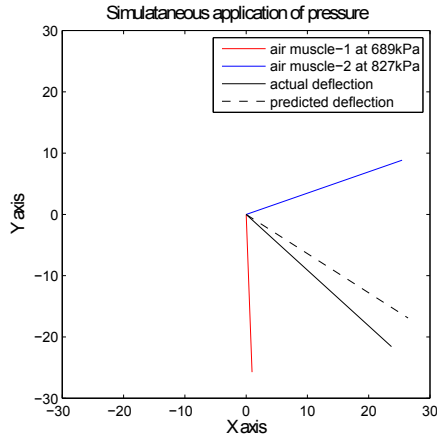
Fig. 13. Experimental vs Theoretical comparison of deflection in random direction
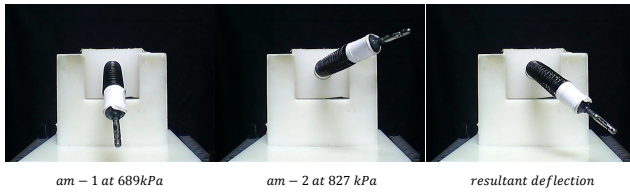

Fig. 14. Deflection in resultant direction

of end-effector as given in section IV.B is then superimposed on this square surface. One unit of thumb stick motion is equal to $\dfrac{\max\{A_i, \|A_i\mathbf{e}_i + A_j\mathbf{e}_j\|\}}{512}$ mm, with $i,j = 1,2,3$. Using this conversion scale, we find the coordinates (v_x, v_y). Once (v_x, v_y) is obtained, sector S_i is found out using the condition $\theta_{vi} + \theta_{vj} = \alpha_j - \alpha_i$; θ_{vi} and θ_{vj} being the angle made by vector $\mathbf{v}$ with the unit vectors $\mathbf{e}_i$ and $\mathbf{e}_j$, respectively. The values a_i and a_j are then calculated using equation (12).
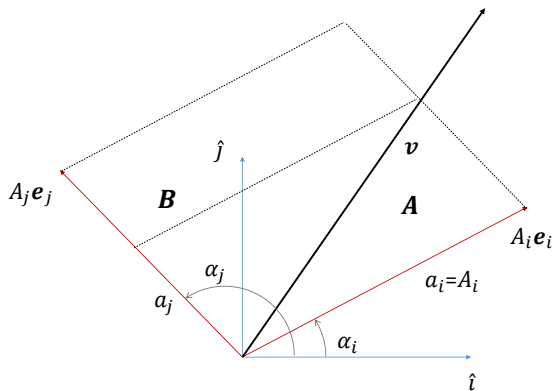

Fig. 15. Vector outside workspace

Since some co-ordinates received from thumb stick lies

outside the workspace of end-effector (see Fig. 15), new co-ordinates are formulated based on the algorithm below:
- Find the subsection (A or B) which vector $\mathbf{v}$ belongs to. The logic used is same as that of finding sectors, except that the vector $\mathbf{e}_j$ is the resultant $\mathbf{e}_i + \mathbf{e}_j$ for section A and $\mathbf{e}_i$ is $\mathbf{e}_i + \mathbf{e}_j$ for section B.
- If $\mathbf{v}$ is in sector A, $a_i = A_i$ (maximum displacement). For calculating a_j, let $\mathbf{e}_v$ be unit vector in the direction of $\mathbf{v}$. From Fig. 15,

$$R\mathbf{e}_v = A_i\mathbf{e}_i + a_j\mathbf{e}_j \qquad (13)$$

- If $\mathbf{v}$ is in sector B, $a_j = A_j$, then

$$R\mathbf{e}_v = a_i\mathbf{e}_i + A_j\mathbf{e}_j \qquad (14)$$

From the above equations, value of R and a_i are calculated.

Once (a_i, a_j) are found out, then equation (12) is solved using *fsolve* function in MATLAB to get the required pressure in both the actuating air muscles.

VI. Results
We performed a large number of experiments to position the tip of a catheter by applying air pressure to three independent air muscles. In this section representative experimental results are shown.

The deflection at the tip of a standard forceps of outer diameter 2.5 mm and length 20 mm from the end-effector tip is measured and plotted. As mentioned earlier, the workspace is divided into three sectors and a point P in workspace can be accessed by applying independent pressure (p_1, p_2, p_3) to the three air muscles $(AM1, AM2, AM3)$, respectively. Fig. 16 shows the end-effector tracing a line in the workspace when a single air muscle is actuated. These are shown by points P_1, P_2 and P_3 (red markers). The applied pressure for each of these points is shown beside the figure. Fig. 16 also shows three representative points P_4, P_5 and P_6 (blue markers) obtained by actuating two air muscles simultaneously. The pressures applied to the two actuators are mentioned beside the figure. Fig. 17, shows that arbitrary positioning of the forceps is possible in the workspace. An approximate circular tip motion of the catheter and the pressures applied to obtain the same is shown in Fig. 17.

VII. Conclusions
A novel end-effector for actuating endoscopic catheters is successfully designed and fabricated. The design uses miniaturized pneumatic artificial muscle of 1.2 mm diameter enabling compactness while delivering required deflection and stiffness. Before analyzing the kinematics of the end-effector, the MPAM used was characterized to find a relation between deflection, pressure and axial load. Even though accurate mathematical models are unavailable for MPAM in literature, a preliminary study shows that cubic fit on experimental data gives a reasonably good initial approximation.
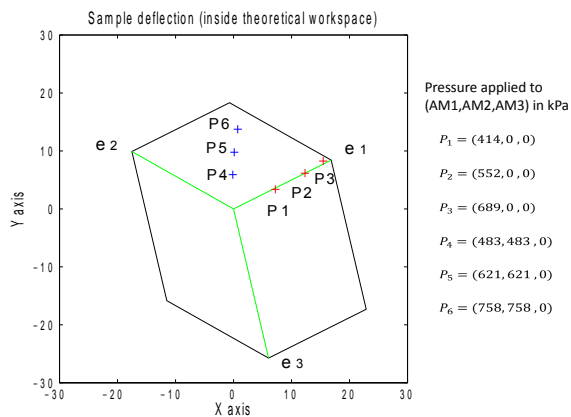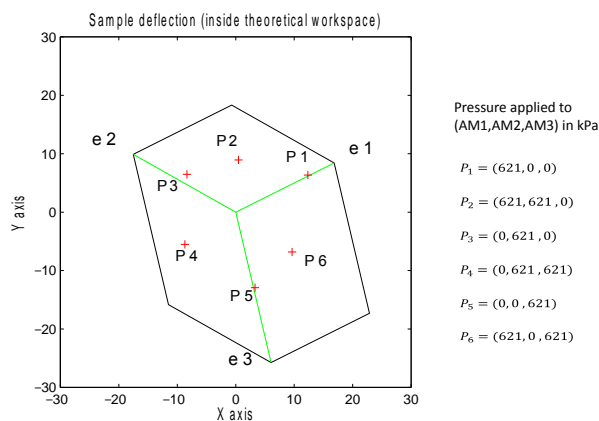
Fig. 16. Tracing line in workspace

Fig. 17. Tracing circle in workspace

The kinematics of the end-effector is studied by actuating single air muscle and then two air muscles simultaneously. Results from air muscle characterization was used to accurately predict the deflection of catheter-less end-effector using elephant trunk robot model. However, an in depth analysis is required for an end-effector with the catheter attached. The fabricated end-effector gives a maximum deflection of up to 26 mm at the tip. The data from single air muscle actuation is then used to extend the analysis to actuation of two air muscles simultaneously. A mathematical formulation has been presented for end-effector kinematics with multiple air muscle actuation. The expected deflection vary from actual value by less than $10°$, which makes the formulation suitable for preliminary analysis and control.

Finally, methodology for implementing actuation in real time by using user input through a thumb stick is discussed. A controller with Arduino board, air compressor, pressure sensors and valves has been developed and it is shown that an end-effector with catheter can be arbitrarily positioned by moving the thumb stick.

The end-effector is in preliminary stages of development and has scope of improvement in terms of making more compact end-effector, finding accurate kinematic and static models and control system implementation for more precise positioning. The authors are currently working towards achieving these goals.

Acknowledgment

References

[1] Baldwin Po Man Yeung and Gourlay, T. A technical review of flexible endoscopic multitasking platforms. *International Journal of Surgery*, 10: 345–354, 2012.

[2] Degani, A., Choset, H., Alon Wolf and A. Zenati, M. A., Highly articulated robotic probe for minimally invasive surgery. In *Proceedings of the 2006 IEEE International Conference on Robotics and Automation*, pp. 4167–4172, Orlando, Florida, May, 2006.

[3] Ikuta, K., Nokata, M. and Aritomi, S., Biomedical micro robots driven by miniature cybernetic actuator. In *Micro Electro Mechanical Systems, MEMS '94, Proceedings, IEEE Workshop on*, pp. 263–268 , Oiso, January 25–28, 1994.

[4] Kai, X., Goldman, R. E., Jienan, D., Allen, P. K., Fowler, D. and Simaan, N., System design of an insertable robotic effector platform for single port access (Spa) surgery. In *International Conference on Intelligent Robots and Systems* , pp. 5546–5552, St. Louis, USA, October 11–15, 2009.

[5] Szewczyk, J., De Sars, V., Bidaud, P., and Dumont, G., An Active tubular polyarticulated micro-system for flexible endoscope. In *Proceedings of ISER2000 (7th International Symposium on Experimental Robotics)*, pp. 179–188, Hawaii, December 10–13, 2000.

[6] Chou, C. P., and Hannaford, B., Measurement and modeling of Mckibben pneumatic artificial muscles. *IEEE Transactions on Robotics and Automation*, 12(1):90–102,February, 1996.

[7] De Volder, M., Moers, A. and Reynaerts, D., Fabrication and control of miniature Mckibben actuators. *Sensors and Actuators A: Physical*, 166(1):111–116, March, 2011.

[8] Tondu, B., Modelling of the McKibben artificial muscle: A review. *Journal of Intelligent Material Systems and Structures*, 23(3):225-253, February, 2012.

[9] Shanthanu, C., Aditya, K., and Ghosal, A., Experimental characterization and control of miniaturized pneumatic artificial muscle. *Journal of Medical Devices*, 8(4):041011, October, 2014.

[10] Parker Miniature valves. *Available: http://ph.parker.com/us/12051/en/vso-miniature-proportional-valve (Date accessed 8/1/2015).*

[11] Arduino. An open-source electronics prototyping platform. *Available: http://www.arduino.cc (Date accessed 9/1/2015).*

[12] Matlab, Version 7.12.0 (R2012a). The MathWorks Inc., Natick, Massachusetts.

[13] Schulte H. F., The characteristics of the McKibben artificial muscle. *The Application of External Power in Prosthetics and Orthotics.National Academy of Sciences*, pp. 94–115., Washington, DC , 1961.

[14] Kydoneifs A. D., Finite Axisymmetric deformations of an initially cylindrical membrane reinforced with inextensible cords. *Quart. Journ, Mech. and Applied Math, Vol. XXIII, Pt.4*, 23(4): 481-488, 1970.

[15] Liu, C. W. and Rahn, R., Fiber-reinforced membrane models of McKibben actuators. *Journal of Applied Mechanics*, 70: 853–859, November, 2003.

[16] Gravange, I. A., Walker, I. D., On the kinematics of remotely-actuated continuum robots. In *Proceedings of the 2000 IEEE International Conference on Robotics & Automation* pp. 2544–2550, San Francisco, CA, April, 2000.